Theor Chem Acc (2001) 105:452–462
DOI 10.1007/s002140000242

Theoretical
Chemistry Accounts

Regular article

A theoretical study of the copper–cysteine bond in blue copper proteins

Ulf Ryde[1], **Mats H. M. Olsson**[1], **Björn O. Roos**[1], **Antonio Carlos Borin**[2]

[1] Department of Theoretical Chemistry, Lund University, P.O.B. 124, 221 00 Lund, Sweden
[2] Instituto de Quìmica, Universidade de São Paulo, Av. Prof. Lineu Prestes 748, 05508-900 São Paulo, SP, Brazil

Received: 7 July 2000 / Accepted: 17 November 2000 / Published online: 21 March 2001

Abstract. The accuracy of theoretical calculations on models of the blue copper proteins is investigated using density functional theory (DFT) Becke's three-parameter hybrid method with the Lee–Yang–Parr correlation functional (B3LYP) and medium-sized basis sets. Increasing the basis set to triple-zeta quality with f-type functions on all heavy atoms and enlarging the model [up to Cu(imidazole-CH_3)$_2$(SC_2H_5) ($CH_3SC_2H_5$)$^{0/+}$] has only a limited influence on geometries and relative energies. Comparative calculations with more accurate wave-function–based methods (second-order Møller–Plesset perturbation theory, complete-active-space second-order perturbation theory, coupled-cluster method, including single and double replacement amplitudes and in addition triple replacement perturbatively) and a variety of basis sets on smaller models indicate that the DFT/B3LYP approach gives reliable results with only a small basis set dependence, whereas the former methods strongly depend on the size of the basis sets. The effect of performing the geometry optimizations in a continuum solvent is quite small, except for the flexible Cu—S_{Met} bond. The results of this study confirm the earlier results that neither the oxidized nor the reduced copper site in the blue proteins is strained to any significant degree (in energy terms) by the protein surrounding.

Key words: Density functional theory – Entatic state theory – Protein strain – Solvation effects – Reorganisation energy

1 Introduction

The blue (or type 1) copper proteins are a group of proteins that exhibit a number of unusual properties, viz. a bright blue color, a narrow hyperfine splitting in the electron spin resonance (ESR) spectra, and high reduction potentials [1–3]. Moreover, the cupric geometry of these proteins is extraordinary: the copper ion is bound to the protein in an approximate trigonal plane formed by a cysteine (Cys) thiolate group and two histidine (His) nitrogen atoms. The coordination sphere in most blue copper sites is completed by one or two axial ligands, typically a methionine (Met) thioether group, but sometimes also a backbone carbonyl oxygen atom or instead an amide oxygen atom from the side chain of glutamine [1, 2, 3, 4].

Several groups of blue copper proteins have been identified, using spectroscopic methods (electronic spectroscopy, resonance Raman, ESR, etc.) in combinations with the determination of the three-dimensional structure of the proteins [1, 2, 3, 4, 5]. The axial type 1 copper proteins, such as plastocyanin, have a short Cu—S_{Cys} bond (around 210 pm), a long Cu—S_{Met} bond (around 290 pm), and no fifth ligand. On the other hand, the rhombic type 1 copper proteins, for example, nitrite reductase, cucumber basic protein, and pseudoazurin, have a longer Cu—S_{Cys} bond (around 215 pm), a shorter Cu—S_{Met} bond (around 260 pm), but still only four ligands. There seems to be a continuous transition between the rhombic and axial copper proteins, which can be described by the angle (φ) between the N_{His}—Cu—N_{His} and the S_{Cys}—Cu—S_{Met} planes. It is 77–89° for plastocyanin, 70–75° for pseudoazurin and cucumber basic protein, and 56–65° for nitrite reductase. In fact, it represents a change in the electronic ground state of the copper complex from a trigonal structure with a pure Cu—S_{Cys} π bond to a tetragonal structure with an increasing σ character in the Cu—S_{Cys} bond. Finally, the azurins are characterized by a fifth ligand, a backbone carbonyl group (which is found at a distance of around 400 pm in the other proteins) and long Cu—S_{Cys}, Cu—S_{Met}, and Cu—O bonds (around 220, 310, and 300 pm, respectively). The structures of the copper site in these three types of copper proteins are compared in Fig. 1 and experimental ranges for the various bonds to the copper ion are compiled in Table 1.

Correspondence to: U. Ryde
e-mail: ulf.ryde@teokem.lu.se

The blue copper proteins serve as electron-transfer agents. Their distorted trigonal geometry is intermediate between the tetrahedral coordination preferred by Cu(I) and the tetragonal geometry of most Cu(II) complexes. As a result, the change in geometry when Cu(II) is reduced to Cu(I) is small [2, 3, 6], which gives a small reorganization energy and allows a high rate of electron transfer [7]. Already in the 1960s it was suggested that the unusual properties of the blue copper proteins are caused by the protein forcing the Cu(II) ion into a coordination geometry more similar to that preferred by Cu(I) [8, 9]. These suggestions were later extended into general theories for metalloproteins, suggesting that a rigid protein may force a metal center into a catalytically poised state, the entatic state [10, 11] and the induced rack theories [12, 13].

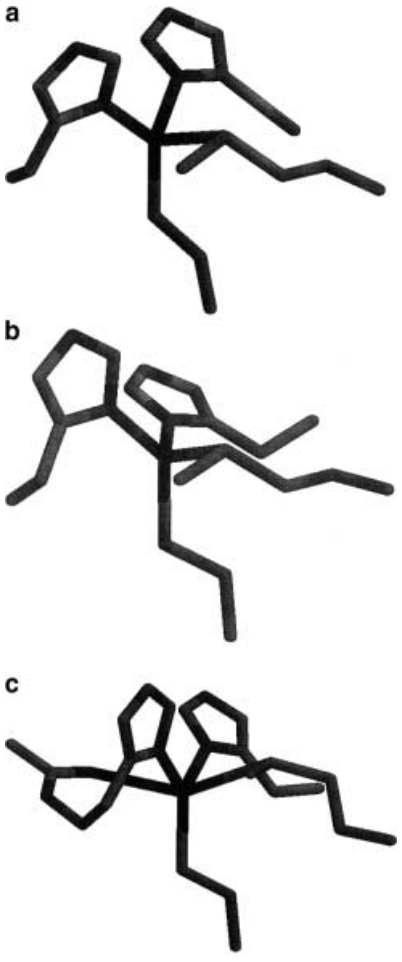

Fig. 1. A comparison of the copper coordination geometry in **a** plastocyanin (an axial type 1 copper protein), **b** nitrite reductase (a rhombic type 1 copper protein), and **c** azurin. The structures are taken from the Brookhaven data bank files 1plc, 1nic, and 4azu [4, 63, 64]

However, these hypotheses have recently been challenged [14, 15]. In particular, it was shown that the optimum geometry of $Cu(Im)_2(SCH_3)(S(CH_3)_2)^+$ (Im = imidazole), a realistic model of the blue copper site in plastocyanin, obtained by accurate quantum chemical calculations is very close to the crystal structure [15]. Equally convincing results were obtained for the optimal structure of $Cu(Im)_2(SCH_3)(OCCH_3NH_2)^+$, a model of the ligand sphere of oxidized stellacyanin [16]. Similarly, we and other groups have shown that most of the differing properties of the blue copper proteins can be explained by the choice of ligands, rather than by protein strain [16–30]. Yet, there are small differences between the optimized models and the experimental structures; for example, the calculated $Cu—S_{Cys}$ distances are too long and the $Cu—S_{Met}$ distances are too short. These differences are especially large for the reduced $Cu(Im)_2(SCH_3)(S(CH_3)_2)$ complex, where the optimum vacuum structure is tetrahedral with a $Cu—S_{Met}$ bond of 237 pm (compared to 290 pm in the protein) [15]. This has been taken as evidence that the $Cu(I)—S_{Met}$ bond is strained by the protein [14, 31, 32].

When the geometry optimizations of the plastocyanin models were performed 6 years ago, they were on the verge of the possible; the calculations took about three months of computing time to complete. Today, such calculations can be done routinely and take less than one week on a standard workstation. Therefore, we now have the opportunity to test whether these calculations converged. In this article we present calculations on several blue copper models, ranging from the minimal $CuSH^{0/+}$ system to the very large $Cu(ImCH_3)_2(SC_2H_5)(CH_3SC_2H_5)^{0/+}$ model. We study the effect of increasing the basis set (up to triple-zeta, TZ, quality with f-type functions on all heavy atoms and even larger for the smallest model) and we also test several theoretical methods of varying sophistication, ranging from Hartree–Fock (HF) to the coupled-cluster method, including single and double replacement amplitudes and in addition triple replacement perturbatively, [CCSD(T)] and complete-active-space second-order perturbation theory (CASPT2). We study how these changes affect

Table 1. Experimental bond lengths and angles in three types of blue copper proteins [15, 29]

Protein	Distance to Cu (pm)			Angle around Cu (°)				φ°
	S_{Cys}	N	S_{Met}	N—N	S_{Cys}—N	S—S	S_{Met}—N	
Plastocyanin, reduced	211–217	203–239	287–292	91–118	110–141	99–114	83–110	74–80
Plastocyanin, oxidised	207–221	189–222	278–291	96–104	112–144	102–110	85–108	77–89
Nitrite reductase, oxidised	208–223	193–222	246–270	96–102	98–140	103–109	84–138	56–65
Azurin[a], reduced	222–231	205–217	321–325	101–104	119–132	109–111	77–94	
Azurin[a], oxidised	212–229	196–213	288–321	98–108	116–138	105–111	84–124	75–87

[a] Azurin has an additional Cu—O bond, which is 319–325 pm in the reduced proteins and 275–316 pm in oxidized proteins

the geometry, the relative energies, and the reorganization energy. Thereby, we can address several issues of functional interest, for example, which is the optimum structure of the blue copper site (trigonal or tetragonal), what is the optimum length of the Cu—S_{Met} bond, and which is the best theoretical method to use on these systems. We also study how the geometry of the copper site changes when the surroundings are modeled as a continuum with a varying dielectric constant. In this way, we gain a deepened understanding of the relation between the structure and function of the blue copper proteins and how they can best be studied by theoretical methods.

2 Methods

Most of our previous quantum chemical geometry optimizations were performed with the density functional B3LYP method (Becke's three-parameter hybrid with the Lee-Yang-Perr correlation functional) [unrestricted formalism for Cu(II)], as implemented in the Turbomole software [33, 34]. This is also the default method in this investigation. For copper, we used the double-zeta (DZ) basis set of Schäfer et al. [35], [62111111/33111/311), enhanced with p-, d-, and f-type functions with exponents 0.174, 0.132, and 0.39 (called DZpdf below). For the other atoms, we employed the 6-31G* basis sets [36]. Larger basis sets were tested, which include DZs2pd2f/6-311(+)G(2d,2p) (DZpdf enhanced by s, p, and f functions with exponents 0.014, 0.462, and 3.55 for copper combined with a valence TZ basis with diffuse functions on S and N, and double polarizing functions on all atoms [36]), and the TZVPP basis [35] (valence TZ basis with a d-type function on H and an f-type function on the other atoms). Only the pure five d and seven f-type functions were used. The full geometry of all models was optimized until the change in energy between two iterations was below 10^{-6} hartree (2.6 J/mol) and the norm of the internal gradients was below 10^{-3} au (0.053 pm or 0.057°). Only the structures with the lowest energy are reported. No symmetry restraints were imposed. Two other density functional methods were also tested, the Becke–Perdew 1986 (BP86) method [37, 38] and the local spin density method (LDA) [39, 40]. In general performance, they are less accurate than B3LYP [41], but they have the advantage of not using HF exchange, which in combination with other techniques can make the calculations about five times faster than B3LYP [42].

The density functional approach was tested by performing calculations on $CuSH^{0/+}$ with the wave-function-based method complete-active-space self-consistent field (CASSCF)/CASPT2 [43–46]. These calculations were performed with the Molcas 4.0 software [47]. Because analytical gradients are not yet implemented for the CASPT2 method, the geometry optimizations for CuSH were performed with a grid in the three degrees of freedom. The optimum geometry was obtained as the minimum of a fitted second-order polynomial and the procedure was repeated until the geometry changed by less than 0.1 pm or 0.1°. In the CASPT2 calculations, generally contracted atomic natural orbital (ANO) basis sets were used [48, 49]. They are compact and optimized to include as much correlation as possible for a given size. Basis sets of four different sizes were tested, as described in Table 2.

In these calculations, the choice of active space is crucial and has turned out to be especially difficult in systems containing a Cu—thiolate bond. From earlier studies it was known that in complexes with first-row transition-metal ions with many 3*d* electrons, the active space should include one correlating orbital for each of the doubly occupied 3*d* orbitals [28, 46]. Therefore the starting active space contains ten orbitals (3*d* and 3*d*′). For the reduced systems, this is the active space used. For oxidized systems, two additional orbitals were included in the active space, one occupied and one correlating S_{Cys} 3*p* orbital, in order to correctly describe the covalence of the Cu—S_{Cys} bond.

Two other correlated methods were also used, second-order Møllet–Plesset perturbation theory (MP2) and CCSD(T). These calculations were performed with the Molcas 4.0 or Gaussian 98 software [47, 50]. All core orbitals were frozen in the MP2, CASPT2, and CCSD(T) calculations, except the Cu 3*s* and 3*p* semicore.

$Cu(Im)_2(SCH)_3(S(CH_3)_2)^{0/+}$ **(1)** has been the standard model for the blue copper proteins. In order to test the effect of enlarging this model, we added a methyl group on each ligand, yielding the $Cu(ImCH_3)_2(SC_2H_5)(S(C_2H_5)(CH_3))^{0/+}$ model **(2)**. For the σ-bonded tetragonal structure, no local minimum can be found with the standard model with density functional methods (it is a transition state). Therefore, we used the slightly smaller $Cu(Im)_2(SH)$-$(S(CH_3)_2)^+$ **(3)** model for these systems, where we removed the methyl group on the Cys ligand model. For this structure, we also tested some models, intermediate in size between models **2** and **3**. For calculations with the more accurate wave-function-based methods two smaller models were used, $CuSH^{0/+}$ **(6)** and $Cu(NH_3)_2$- $(SH)(SH_2)^{0/+}$ **(7)**. The various structures are illustrated in Fig. 2.

The inner-sphere reorganization energy was estimated in the same way as for the blue copper proteins [26]. The reorganization energy for the oxidized complex (λ_{ox}) was calculated as the difference in energy between the oxidized complex at its optimal geometry and at the optimal geometry of the reduced complex. Likewise λ_{red} was calculated as the energy of the reduced complex at its optimal geometry minus the energy of the reduced complex calculated at the geometry optimal for the oxidized complex. The total inner-sphere reorganization energy for a self-exchange reaction (λ_i) is the sum of λ_{ox} and λ_{red}. In contrast to the outer-sphere reorganization energy, the inner-sphere reorganization energy is independent of the geometry of the complex between actual donor and acceptor and, therefore, has a functional significance [29]. One should keep in mind, however, that the reorganization energy computed in this way is based on a simplistic model of the electron-transfer reaction, which may not always be valid.

Solvation effects were studied using the conductor polarizable continuum model as implemented in the Gaussian 98 software [51, 52] using the B3LYP method and the DZpdf basis sets (full geometry optimizations). In this method, the molecule is placed in a cavity formed by overlapping atom-centered spheres surrounded by a dielectric medium. The induced polarization of the surroundings is represented by point charges distributed on the surface of the

Table 2. Basis sets used (uncontracted/contracted)

Basis set	Cu	C, N, O	S	H
DZpdf/6-31G*	14s10p6d1f/8s6p4d1f	10s4p1d/3s2p1d	16s10p1d/4s3p2d	4s/2s
DZs2pd2f/ 6-311(+)G(2d,2p)	15s11p6d2f/9s7p4d2f	12s6p2d/5s4p2d	14s10p2d/7s6p2d	5s2p/3s2p
TZVPP	17s11p6d1f/6s4p3d1f	11s6p2d1f/ 5s3p2d1f	14s9p2d1f/ 5s5p2d1f	5s2p1d/3s2p1d
ANO-S	17s12p9d4f/6s4p3d2f	–	13s10p4d/4s3p2d	7s3p/2s1p
ANO-L1	21s15p10d6f4g/6s5p4d3f2g	–	17s12p5d4f/ 5s4p3d2f	8s4p3d/3s2p1d
ANO-L2	21s15p10d6f4g/7s6p5d4f3g	–	17s12p5d4f/ 6s5p4d3f	8s4p3d/3s2p1d

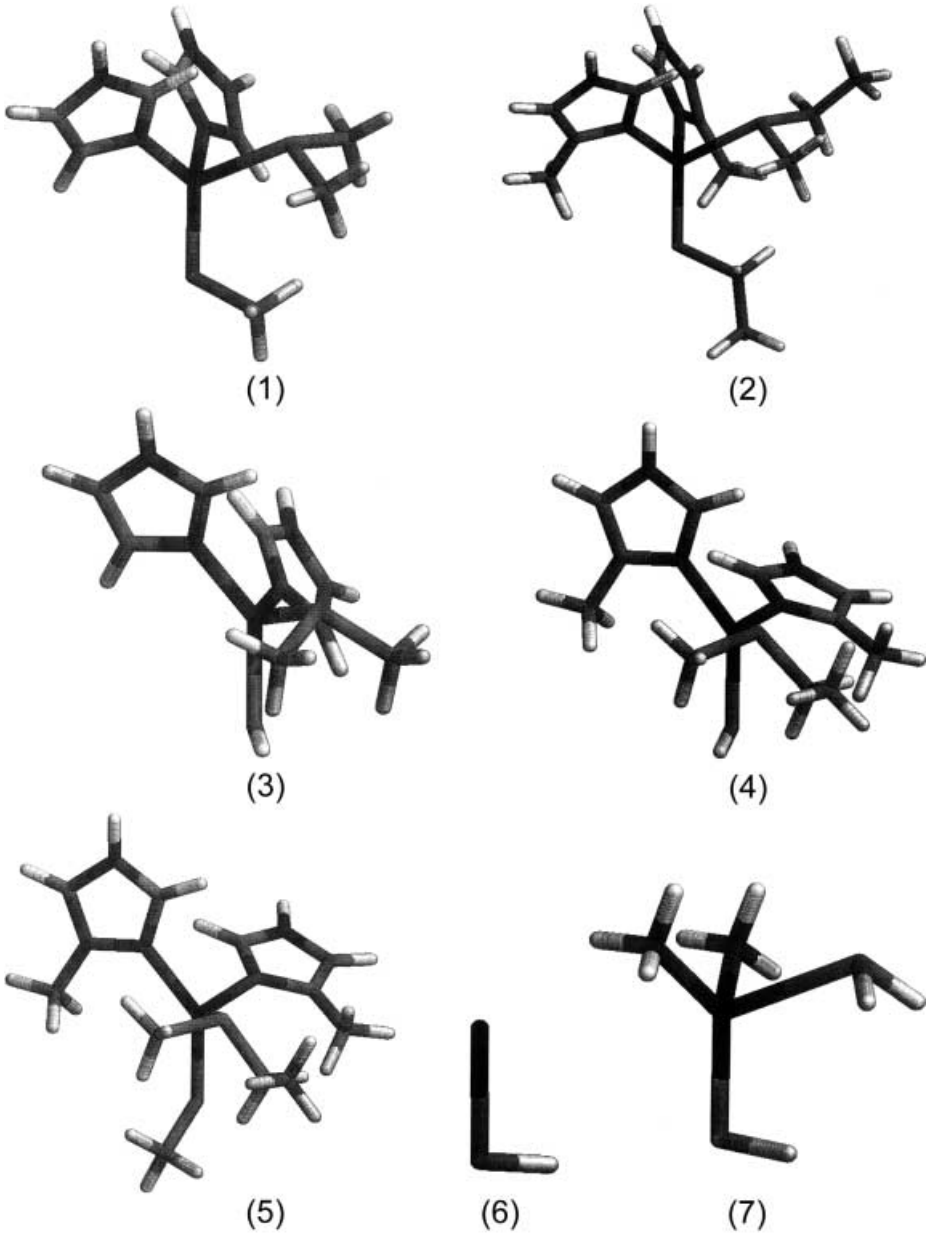

Fig. 2. The seven models used in the calculations:
1, $Cu(Im)_2$ $(SCH_3)(S(CH_3)_2)^+$;
2, $Cu(ImCH_3)_2(SC_2H_5)(S(CH_3)(C_2H_5))^+$;
3, $Cu(Im)_2(SH)(S(CH_3)_2)^+$;
4, $Cu(ImCH_3)_2(SH)(S(CH_3)(C_2H_5))^+$;
5, $Cu(ImCH_3)_2(SCH_3)(S(CH_3)(C_2H_5))^+$;
6, $CuSH^+$; and
7, $Cu(NH_3)_2(SH)(SH_2)^+$.
The lowest optimum structure for the oxidized state of each complex is shown

cavity and the field of these charges polarizes the electrons of the solvated molecule. In this way, solvation effects are included in a self-consistent manner. In addition to this electrostatic energy, the method also includes cavitation, dispersion, and exchange solute–solvent terms [53–55]. For the atom-centered spheres, we used default atomic radii, i.e. those obtained according to the united atom model for HF strategy [56], where the radii depend on the hybridization and substituents on each of the atoms. The hydrogen atoms are included in the radii of the heavier atoms, to make the cavity surface smoother. This approach has been thoroughly tested and has been shown to give good results compared to experiments [56]. In order to improve the description of the cavity surface and charges induced by the solvent, a smaller than default area of each surface element was used, 0.4 $Å^2$. Unfortunately, these calculations did not converge for the oxidized complexes.

In order to establish if the calculated geometries represent true equilibrium structures, frequencies were calculated for some of the optimized complexes with the Gaussian 98 software [50]. All calculations were run on SGI Origin 2000 or on Octane workstations and on IBMSP2 machines.

3 Results and discussion

3.1 The CuSH model

We first discuss the results obtained for the $CuSH^{0/+}$ model. The emphasis here is the comparison of the density functional approach and the accurate wave-function-based models. CuSH is a minimal model of the copper–cysteinate interaction that has proved to be indispensable for the unusual properties of the blue copper proteins. For this small model, we can use large basis sets and accurate methods. We studied three different states of the molecule. The lowest energy state in the two irreps of C_s were studied for the oxidized Cu(II) complex. The $^2A''$ state is a representative for the axial type 1 copper proteins, such as plastocyanin and azurin, whereas the $^2A'$ state is a model of the rhombic

type 1 proteins, exemplified by nitrite reductase and pseudoazurin. For the reduced complex Cu(I), only the lowest energy state, of $^1A'$ symmetry, was studied.

The geometry of the $^2A''$ state of $CuSH^+$ calculated with several different methods (but with the same basis set, ANO-S) is shown in Table 3. Both the HF and CASSCF methods give too long Cu—S bonds and too short S—H bonds and also a somewhat too large angle. The results of the other methods are, on the other hand, similar. Of the three density functional methods, the LDA gives the shortest and B3LYP the longest Cu—S bond, whereas the result of BP86 is intermediate. The value of B3LYP with the ANO-S basis set is still almost 2 pm shorter than result obtained with the wave-function-based methods. The opposite trend applies for the S—H bond, and again the B3LYP result seems to be the most reliable. The Cu—S—H angle increases for the three methods, and the B3LYP result is very close to the ab initio results.

The wave-function-based methods [MP2, CASPT2, and CCSD(T)] give the same result, within 2 pm and 2°. The similarity between the results of the MP2 and CASPT2 methods indicates that the system is not especially multiconfigurational in nature. This is confirmed by the weight of the major configuration state function, which is 0.96.

The convergence of the geometry with respect to the basis sets for the B3LYP, MP2, and CASPT2 methods is shown in Table 4. The B3LYP results seem to be stable: the bond lengths change by less than 1.1 pm and the angle by less than 0.3° when the basis set is varied from the standard DZpdf/6-31G* basis set, and the latter results can be considered as practically converged. For the CASPT2 method, the results are quite different. The Cu—S distance decreases by 5 pm when going from ANO-S to ANO-L2, and even between the two large ANO-L basis sets there is a difference in this distance of almost 2 pm. The S—H and Cu—S—H angles are more stable, but the S—H distance also changes by 1.1 pm when going from ANO-S to ANO-L1. The results obtained with the extended ANO-L2 basis set can considered as practically converged with respect to a further increase in the basis set and can therefore be used as an indication of the error obtained with the smaller basis sets and other methods. Comparing the other methods with the CASPT2/ANO-L2 results, one concludes that B3LYP is the best method for the S—H bond and the Cu—S—H angle, whereas BP86 gives a slightly better result for the Cu—S distance. B3LYP gives somewhat shorter (and thus improved) Cu—S distances than MP2, CASPT2, and CCSD(T) with the ANO-S basis set. As expected, MP2 shows a similar basis set dependence as CASPT2.

Next, we studied the $^2A'$ state of $CuSH^+$. The results in Table 5 are similar to those of the $^2A''$ state. CASPT2 shows a strong basis set dependence, with an 8 pm decrease in the Cu—S bond length when going from ANO-S to ANO-L2. The three density functionals behave in the same way as for the $^2A''$ state, and the CASPT2 result for the Cu—S bond length with the largest basis set is between the results of B3LYP and BP86. However, for the Cu—S—H angle, the three density functional methods predict an angle (113–115°) that is almost 20° smaller than what is obtained with the three correlated methods (132–138°). The reason for this behavior is not clear, but a calculation with the CCD method shows that is not caused by problems in the perturbation method.

It is interesting to note that the $^2A'$ state of $CuSH^+$ is around 90 kJ/mol less stable than the $^2A''$ state (86 kJ/mol with CASPT2/ANO-L2 and 93 kJ/mol with CCSD(T)/ANO-S), whereas the corresponding tetragonal state for the more realistic blue copper protein models is virtually degenerate (within 7 kJ/mol) to the trigonal state (corresponding to the $^2A''$ state), which reflects the inherent stability of the Cu—S bonds involved in the two complexes. In the $^2A''$ state, there is a π bond between a S 3*p* orbital and two lobes of a Cu 3*d* orbital. In the $^2A'$ state, on the other hand, there is a σ bond instead. The π bond is inherently slightly shorter and appreciably stronger than the σ bond; however, addition of more ligands to the complex changes the relative energies of the two states. For the σ-bonded

Table 3. The structure of the $^2A''$ state of $CuSH^+$, optimized with various methods and the ANO-S basis set (distances in picometers and angles in degrees)

Method	Cu—S	S—H	Cu—S—H
HF	243.1	133.5	100.1
CASSCF	236.7	134.0	100.6
LDA	207.8	137.3	95.1
BP86	213.3	136.8	95.8
B3LYP	217.7	135.5	97.0
MP2	218.7	135.7	98.2
CCSD(T)	219.2	136.2	96.9
CASPT2	219.5	135.7	97.5
CASPT2/ANO-L2	214.8	134.6	97.9

Table 4. Basis set convergence for the geometry of the $^2A''$ state of $CuSH^+$, optimized with the B3LYP, MP2, and CASPT2 methods

Basis set	Cu—S			S—H			Cu—S—H		
	B3LYP	MP2	CASPT2	B3LYP	MP2	CASPT2	B3LYP	MP2	CASPT2
6-31G*	217.7	217.1	–	136.0	134.7	–	97.1	98.6	–
6-311(+) G(2d,2p)	217.1	217.1	–	135.5	134.3	–	96.7	98.2	–
TZVPP	218.0	219.3	–	135.8	134.5	–	97.1	98.9	–
ANO-S	217.7	218.7	219.9	135.5	135.6	135.7	97.0	98.2	97.4
ANO-L1	–	–	216.6	–	–	134.6	–	–	97.7
ANO-L2	216.6	–	214.8	135.5	–	134.6	97.2	–	97.9

state, three other ligands may form σ bonds with the other three lobes of the Cu 3*d* orbital. For the π-bonded state, on the other hand, two lobes of the Cu 3*d* orbital are already occupied for the π bond, so only two other ligands can form strong bonds to the copper ion. Additional ligands would become weakly bound axial ligands (such as the Met ligand in the axial blue copper proteins). Therefore, with four or more ligands, the σ-bonded state will be stabilized, leading to the near degeneracy in the blue copper ligand sphere. With harder ligands than thiolate, the π-bonded state will be even more destabilised, explaining why most Cu(II) complexes are tetragonal with four σ-bonded ligands [26].

Finally, we also studied the ground state of the reduced CuSH complex. The geometry of this complex calculated with different methods is shown in Table 6. The result is very similar to that of the other two systems. As expected (c.f. Table 7), the correlated methods are more sensitive to the basis sets, with 3- and 1.3-pm decreases in the Cu—S and S—H bond lengths. Interestingly, B3LYP is the density functional method that performs best for the S—H bond and the Cu—S—H angle, whereas it gives a 7-pm too long Cu—S bond length. For the latter bond, actually the LDA method seems to give the best estimate (compared to the CASPT2 method with the largest basis set).

The angle in CuSH is smaller than in the positive ion, indicating a more covalent bonding situation where the copper atom binds to the π orbital of the SH radical. This also explains the slightly shorter bond distance.

In conclusion, the calculations on the CuSH model indicate that MP2, CASPT2, and CCSD(T) all give quite similar results. The geometrical parameters are only converged with extended basis sets as the CASPT2 results with the ANO-L2 basis shows. Among the density functional methods used in this study, B3LYP seems to give the most reliable result. However, for the Cu—S bond, the result varies for the three complexes, and B3LYP often gives too long a bond.

Table 5. The structure of the $^2A'$ state of $CuSH^+$, optimized with various methods and the ANO-S basis set (distances in picometers and angles in degrees)

Method	Cu—S	S—H	Cu—S—H
HF	253.6	133.0	142.4
LDA	207.6	136.4	115.0
BP86	213.6	136.0	112.8
B3LYP	217.2	134.9	114.4
MP2	221.8	134.9	138.3
CCSD(T)	221.9	135.4	133.0
CASPT2	223.4	135.1	135.6
CASPT2/ANO-L2	215.4	134.0	131.7

Table 6. The structure of neutral CuSH, optimized with various methods and the ANO-S basis set (distances in picometers and angles in degrees)

Method	Cu—S	S—H	Cu—S—H
HF	223.8	133.6	96.5
LDA	206.0	136.3	92.7
BP86	211.1	135.8	93.6
B3LYP	214.0	134.6	94.4
MP2	210.2	135.2	94.7
CCSD(T)	216.0	135.6	94.2
CASSCF	223.8	134.0	93.5
CASPT2	210.3	135.2	94.4

3.2 Models of the blue copper proteins

Next, we turned to a more realistic model of the blue copper proteins, $Cu(Im)_2(SCH_3)S(CH_3)_2)^{+/0}$ (**1**). The results of improving the basis sets or the model system or changing the quantum chemical method for five different systems are shown in Tables 8, 9, 10, 11, and 12. For the reduced system, we studied the optimum geometry and a structure with the $Cu—S_{Met}$ bond length constrained to 290 pm (a typical value in the crystal structures of these proteins). For the oxidized complex, we studied the optimum trigonal geometry (a model of the axial blue copper proteins, e.g. plastocyanin) and an alternative configuration where imidazole is the axial ligand instead of the Met model. For the oxidized complex, we also studied a tetragonal structure (a model of the rhombic type 1 copper proteins, such as nitrite reductase). However, this structure cannot be found with the standard model **1**. Therefore, we used instead the smaller $Cu(Im)_2(SH)(S(CH_3)_2^+$ model (**2**), where the methyl group on the Cys model has been removed. For that model the tetragonal structure is the ground state, whereas the trigonal structure is a transition state [25].

For the oxidized complexes, the results are very stable. If the basis set is enhanced to the appreciably larger DZs2pd2f/6-311(+)G(2d,2p) or TZVPP basis sets (the latter basis set gives 755 basis functions), the bond lengths to copper change by less than 2 pm and the angles by less than 1°. For the reduced complex, the

Table 7. Basis set convergence for the geometry of neutral CuSH, optimized with the B3LYP, MP2, and CASPT2 methods

Basis set	Cu—S			S—H			Cu—S—H		
	B3LYP	MP2	CASPT2	B3LYP	MP2	CASPT2	B3LYP	MP2	CASPT2
6-31G*	214.1	209.8	–	135.6	134.7	–	93.9	93.9	–
6-311(+) G(2d,2p)	213.6	209.9	–	134.6	133.7	–	94.3	94.0	–
TZVPP	213.5	209.9	–	135.0	133.9	–	94.3	94.3	–
ANO-S	214.0	210.2	210.3	134.6	135.2	135.2	94.4	94.7	94.4
ANO-L2	213.1	207.9	207.2	134.6	133.9	133.9	94.5	94.6	94.0

Table 8. The effect of the model size, basis set, and theoretical method on the geometry of trigonal models of the oxidized blue copper site

Method	Model[a]	Basis[b]	Distance to Cu (pm)			Angle around Cu (°)				φ°
			S_{Cys}	N	S_{Met}	N—N	S_{Cys}—N	S—S	S_{Met}—N	
HF	**1**	1	226	205,207	270	101	107,134	114	95,100	83.6
BP	**1**	1	219	203,210	236	103	102,130	116	99,105	81.1
B3LYP	**1**	1	218	204,205	267	103	119,122	117	94,95	89.1
B3LYP	**1**	2	219	206	269	104	119,122	117	94,96	88.5
B3LYP	**1**	3	218	205	267	103	118,123	117	94,96	88.3
B3LYP	**2**	1	218	204,206	271	102	120,125	115	94,95	89.7

[a] Models: **1**, $Cu(Im)_2(SCH_3)(S(CH_3)_2)^+$; **2**, $Cu(ImCH_3)_2(SC_2H_5)(S(CH_3)(C_2H_5))^+$
[b] Basis sets: 1, DZpdf/6-31G*; 2, TZVPP; 3, DZs2pd2f/6-311(+)G(2d,2p)

Table 9. The effect of the model size, basis set, and theoretical method on the geometry of trigonal models of the oxidized blue copper site with one imidazole group as the axial ligand

Method	Model[a]	Basis[b]	Distance to Cu (pm)			Angle around Cu (°)				φ°
			S_{Cys}	N	S_{Met}	N—N	S_{Cys}—N	S—S	S_{Met}—N	
BP	**1**	1	219	203,210	236	102	102,130	116	99,106	80.8
B3LYP	**1**	1	220	204,214	243	102	102,132	114	99,104	81.2
B3LYP	**1**	2	220	205,216	245	102	102,132	115	99,103	82.2
B3LYP	**1**	3	219	205,214	242	101	101,132	115	99,105	81.2
B3LYP	**2**	1	220	206,215	246	102	108,123	118	99,106	83.3

[a] Models: **1**, $Cu(Im)_2(SCH_3)(S(CH_3)_2)^+$; **2**, $Cu(ImCH_3)_2(SC_2H_5)(S(CH_3)(C_2H_5))^+$
[b] Basis sets: 1, DZpdf/6-31G*; 2, TZVPP; 3, DZs2pd2f/6-311(+)G(2d,2p)

Table 10. The effect of the model size, basis set, and theoretical method on the geometry of tetragonal models of the oxidized blue copper site

Method	Model[a]	Basis[b]	Distance to Cu (pm)			Angle around Cu (°)				φ°
			S_{Cys}	N	S_{Met}	N—N	S_{Cys}—N	S—S	S_{Met}—N	
MP2	**1**	1	217	199,210	239	96	98,141	112	95,115	70
BP	**3**	1	222	203,210	236	100	98,139	104	95,125	64
B3LYP	**3**	1	223	205,214	242	100	98,141	103	95,126	62
B3LYP	**3**	2	223	206,216	244	100	98,141	103	95,125	63
B3LYP	**3**	3	222	205,214	241	99	97,140	103	95,126	63
B3LYP	**4**	1	223	206,206	241	98	97,142	103	93,131	58
B3LYP	**5**	1	221	206,211	242	98	98,139	111	94,117	69
B3LYP	**2**	1	221	206,212	242	98	99,123	112	94,115	70

[a] Models: **1**, $Cu(Im)_2(SCH_3)(S(CH_3)_2)^+$; **2**, $Cu(ImCH_3)_2(SC_2H_5)(S(CH_3)(C_2H_5))^+$; **3**, $Cu(Im)_2(SH)(S(CH_3)_2)^+$; **4**, $Cu(ImCH_3)_2(SH)(S(CH_3)(C_2H_5))^+$; **5**, $Cu(ImCH_3)_2(SCH_3)(S(CH_3)(C_2H_5))^+$
[b] Basis sets: 1, DZpdf/6-31G*; 2, TZVPP; 3, DZs2pd2f/6-311(+)G(2d,2p)

Table 11. The effect of the model size, basis set, and theoretical method on the geometry of models of the reduced blue copper site (fully optimized geometry)

Method	Model[a]	Basis[b]	Distance to Cu (pm)			Angle around Cu (°)				φ°
			S_{Cys}	N	S_{Met}	N—N	S_{Cys}—N	S—S	S_{Met}—N	
HF	**1**	1	238	225,226	283	114	112,112	109	99,111	85.3
MP2	**1**	1	223	205,208	220	104	103,108	114	106,119	88.2
BP	**1**	1	230	209	228	109	104,107	111	111,116	89.8
B3LYP	**1**	1	232	214,215	237	109	105,107	113	107,114	88.7
B3LYP	**1**	2	232	216	239	107	105,107	116	109,112	89.8
B3LYP	**1**	3	231	215,217	234	105	104,107	116	111,112	88.3
B3LYP	**2**	1	231	211,221	239	102	106,114	112	108,114	89.2

[a] Models: **1**, $Cu(Im)_2(SCH_3)(S(CH_3)_2)^+$; **2**, $Cu(ImCH_3)_2(SC_2H_5)(S(CH_3)(C_2H_5))^+$
[b] Basis sets: 1, DZpdf/6-31G*; 2, TZVPP; 3, DZs2pd2f/6-311(+)G(2d,2p)

changes are somewhat larger, 3 pm in the bond lengths and 4° for the angles. However, the reduced complex with a fixed Cu—S_{Met} bond behaves differently. There, a imidazole group tends to dissociate when the basis set is increased [it dissociates fully with the TZVPP basis set and it binds at a 15 pm larger distance with the DZs2pd2f/6-311(+)G(2d,2p) basis set]. This reflects that the reduced complex is very flexible and that there is a find-tuned equilibrium between four- and three-coordinate states (reflecting that the Cu—S_{Met}

Table 12. The effect of the model size, basis set, and theoretical method on the geometry of models of the reduced blue copper site with the Cu—S_{Met} distance kept fixed at 290 pm

Method	Model[a]	Basis[b]	Distance to Cu (pm)		Angle around Cu (°)				φ°	Relative energy (kJ/mol)
			S_{Cys}	N	N—N	S_{Cys}—N	S—S	S_{Met}—N		
BP	**1**	1	221	199,209	110	113,130	96	97,103	89.3	10.7
MP2	**1**	1	220	197,200	128	111,117	101	93,96	87.8	20.6
B3LYP	**1**	1	227	205,210	119	112,120	99	100,101	88.0	4.4
B3LYP	**1**	3	223	203,225	102	103,110	98	97,102	88.8	4.4
B3LYP	**2**	1	224	204,220	104	111,135	99	98,102	88.0	3.7

[a] Models: **1**, $Cu(Im)_2(SCH_3)(S(CH_3)_2)^+$; **2**, $Cu(ImCH_3)_2(SC_2H_5)(S(CH_3)(C_2H_5))^+$
[b] Basis sets: 1, DZpdf/6-31G*; 2, TZVPP; 3, DZs2pd2f/6-311(+)G(2d,2p)
[c] The energy compared to the complex fully optimized with the same method

interaction is of similar strength as a NH—S_{Met} hydrogen bond).

Somewhat larger changes are observed when a methyl group is added to all ligands [i.e. $Cu(ImCH_3)_2(SC_2H_5)(S(CH_3)(C_2H_5))^+$, **2**], up to 4 pm in the bond length and 9° in the angles for the oxidized complexes. Again, in the reduced complexes, one of the Im groups showed a tendency to dissociate, with increases in the Cu—N distance of up to 11 pm and differences of up to 15° in the angles. Furthermore, the tetragonal complex [for which we used the $Cu(Im)_2(SH)(S(CH_3)_2)^+$ model, **3**] behaves differently. When methyl groups were added to the His and Met models [$Cu(ImCH_3)_2(SH)(S(CH_3)(C_2H_5))^+$, **4**], the geometry changes very little (less than 1 pm and 5°); however, if a methyl or ethyl group is added to the Cys model (**5** or **2**), the structure change significantly, as is flagged by a 6–8° increase in the φ angle (φ is the angle between the S_{Cys}—Cu—S_{Met} and the S_{Met}—Cu—N plane; it is around 90° in a trigonal structure and less than around 75° in a tetragonal structure). This indicates that the geometry goes toward a trigonal structure.

Yet, with the largest model [$Cu(ImCH_3)_2(SC_2H_5)(S(CH_3)(C_2H_5))^+$, **2**], a structure is obtained that is clearly different from the two trigonal structures obtained with the same model, even if 10-times tighter convergence criteria are used in the geometry optimizations, and a frequency calculation shows that all three structures are true local minima. Interestingly, the three structures have the same energy within 4 kJ/mol (the trigonal one is the most stable, the one with an axial Im group the least). The zero-point energy does not change this situation significantly, whereas thermodynamic corrections (at ambient temperature and pressure) increase the energy difference to 8 kJ/mol, keeping the order. The distortion coordinate between the trigonal and tetragonal structure consists mainly of the angle between the N—Cu—N and S—Cu—S planes [26]. It is hard to discern this mode in the vibrational spectrum, but there are about ten lines below 100 cm^{-1} (1.2 kJ/mol), several of which contain such a component. This also shows that there is a finite barrier between the two states, even if the zero-point energy is taken into account. Altogether, this illustrates the plasticity of the blue copper site.

It is not only interesting to study variations in the geometry, but also in energy. The energy difference between the reduced model in its optimal geometry and with the Cu—S_{Met} bond length fixed at 290 pm hardly changes at all when the basis set or model system is changed, less than 1 kJ/mol. However, the difference between the oxidized model in the trigonal structure and the structure with an axial imidazole group changes by 6 kJ/mol both when the basis set is increased and when the model is increased. In fact, the structure with an axial imidazole is most stable with the normal model (by 3 kJ/mol), whereas the trigonal structure is more stable with the large model system. Enlargement of the basis set changes the energy in the other direction, but much more for the DZs2pd2f/6-311(+)G(2d,2p) basis than for TZVPP (less than 1 kJ/mol). Therefore, our standard method can be predicted to give quite accurate results owing to a fortuitous cancelation of errors.

It is even more interesting to study how the inner-sphere reorganization energies vary with the basis sets and model systems [27]. The result in Table 13 shows that the total reorganization energy does not change if the model system is enlarged; however, the individual energies (λ_{ox} and λ_{red}) change by 3 kJ/mol. When the basis set is enlarged, the reorganization energy changes by 4–7 kJ/mol, either up or down, depending on the basis set. BP86 gives a 6 kJ/mol lower reorganization energy than B3LYP, whereas MP2 gives larger values. We also studied the reorganization energy for the CuSH system, but this energy is very low, less than 3 kJ/mol. It does not vary very much with the different methods. For example, the CASPT2 and B3LYP results differ by less than 2 kJ/mol.

It would be interesting to check if the results converge also with respect to the method. Unfortunately, there is no method that is more accurate than B3LYP and that can be used for models of this size. Coupled-cluster methods cannot be used for these large systems and it is still not possible to do analytical geometry optimizations with the CASPT2 method. However, for the $CuSH^{+/0}$ system, the MP2 calculations gave results in agreement with the more accurate methods, at least with large basis sets. Moreover, for Zn^{2+} complexes (which are isoelectronic with Cu^+), B3LYP and MP2 give virtually identical results [57]. Therefore, we did calculations with the MP2 method for the two reduced and one oxidized systems in Tables 10, 11, and 12. The resulting MP2 structures differed from the B3LYP results by up to 17 pm and 9° in the bond lengths and angles, respectively. These appreciable differences led us to study the MP2 method more closely for the intermediate $Cu(NH_3)_2(SH)(SH_2)$ model. The results in Table 14

show that the MP2 results for the Cu—S_{Cys} bond are reasonably stable with respect to basis set changes and are slightly shorter than the B3LYP result. The Cu—N distance shows more irregular behavior, but the result obtained with the largest basis set (TZVPP) is rather close to the B3LYP distance. The weak Cu—S_{Met} bond is consistently somewhat shorter at the MP2 level of theory. The general conclusion is that since the MP2 results obtained with the largest basis set are close to the B3LYP results, the latter method can safely be used to study the structural properties of these systems. Interestingly, the tetragonal MP2 structure for the oxidized complex is very similar to the structure obtained with the largest model **2** [$Cu(ImCH_3)_2(SC_2H_5)(S(CH_3)(C_2H_5))^+$] and, therefore, is quite different from the B3LYP structure with the same model and basis set.

Finally, we also studied another density functional method, BP86. The results in Tables 8, 9, 10, 11, and 12 show that the change in density functional leads to quite appreciable changes in the geometry, up to 10° in the angles and 9 pm for the bond lengths. The trigonal oxidized structure could not even be found with the BP86 method; these calculations ended up in the structure with an axial imidazole group. The BP86 structures are significantly less similar to the experimental structures than the B3LYP structures. Moreover, the BP86 energy differences differ from those of B3LYP by at least 7 kJ/mol. Therefore we cannot recommend this method for general use.

In conclusion, it seems that the results at our normal level of theory, B3LYP//DZpdf/6-31G*, are reasonably converged, both with respect to geometries and energies. However, it must be recognized that the systems are extremely flexible with many alternative configurations. The relative energies of these configurations strongly depend on the models used, and we can still not decide whether the optimal geometry of the oxidized blue copper site is trigonal or tetragonal. It is clear, however, that the energy difference is very small, less than 7 kJ/mol.

Table 13. The effect of the model size, basis set, and theoretical method on the reorganization energy of the trigonal plastocyanin model (reduced state fully relaxed)

Method	Model[a]	Basis[b]	Reorganization energy (kJ/mol)		
			λ_{red}	λ_{ox}	λ_{tot}
B3LYP [15]	**1**	1	32.7	28.8	61.5
B3LYP	**1**	2	30.6	27.2	57.8
B3LYP	**1**	3	28.4	40.6	68.9
B3LYP	**2**	1	29.8	31.4	61.2
BP86	**1**	1	24.5	30.9	55.4
MP2	**1**	1	46.8	50.5	97.3

[a] Models: **1**, $Cu(Im)_2(SCH_3)(S(CH_3)_2)^+$; **2**, $Cu(ImCH_3)_2(SC_2H_5)(S(CH_3)(C_2H_5))^+$
[b] Basis sets: 1, DZpdf/6-31G*; 2, TZVPP; 3, DZs2pd2f/6-311(+)-G(2d,2p)

Table 14. The effect of the basis set on the geometry of the reduced $Cu(NH_3)_2(SH)(SH_2)$ model (**7**) studied with the MP2 method, assuming C_s symmetry. The B3LYP result is also included for comparison

Basis	Distance to Cu (pm)			Angle around Cu (°)			
	S_{Cys}	N	S_{Met}	N—N	S_{Cys}—N	S—S	S_{Met}—N
DZpdf/6-31G*	224	215	220	104	99	128	112
cc-pVDZ	225	201	209	107	91	130	116
aug-cc-pVDZ	227	198	211	106	96	121	117
TZVPP	228	224	229	106	95	140	109
B3LYP[a]	232	221	234	111	98	128	110

[a] Basis set: DZpdf/6-31G*

3.3 Solvation effects

When we studied how the reduction potential depends on the length of the Cu—S_{Met} bond, our results indicated that the geometry of the blue copper models may change quit appreciably when solvation effects are taken into account [28]. We therefore performed a number of geometry optimizations of the $Cu(Im)_2(SCH_3)(S(CH_3)_2)$ (**1**) complex in a dielectric continuum characterized by various values of the dielectric constant. The effective dielectric constant inside a protein is usually assumed to be 2–16, but large variations are found in different proteins [58–60]. The active site in the blue copper proteins is buried, except for one of the His ligands, which reach the surface of the protein. Both the Cys sulphur and the non-coordinating nitrogen atoms of the Im groups form hydrogen bonds in the crystal structures, but there are no buried water molecules close to

Table 15. The effect of the dielectric constant on the geometry of the $Cu(Im)_2(SCH_3)(S(CH_3)_2)$ complex (**1**). The calculations were performed with the B3LYP method, the DZpdf/6-31G* basis set, and the conductor polarizable continuum solvation model with a water probe. The Gaussian 98 software was used

ϵ	Distance to Cu (pm)			Angle around Cu (°)				φ°
	S_{Cys}	N	S_{Met}	N—N	S_{Cys}—N	S—S	S_{Met}—N	
1	232	214,215	237	109	105,108	115	107,113	89.4
2	233	209,211	240	116	106,108	106	103,115	87.0
4	234	209,211	241	117	107,109	105	103,114	86.8
8	233	209,210	244	118	108,112	106	100,112	86.7
16	235	208,208	246	120	108,110	104	103,110	87.6
80	232	208,211	248	112	108,121	104	98,110	87.4

the copper site [1, 2]. Therefore, we investigated a full range of dielectric constants from 1 (vacuum) to 80 (water solution), so the actual value should be included and general trends can be seen. The results in Table 15 show that the bond lengths change by up to 11 pm and the angles by up to 13°. Thus, the geometry changes with the dielectric surrounding, but the effects are not very large (appreciably smaller than the earlier single-point results indicated [28]) and the general geometry is not changed (the φ angle does not decrease below 86°).

It is notable that the largest effect is seen for the $Cu—S_{Met}$ bond length, which increases with the dielectric constant. Thus, solvent effects may explain some of the difference between the optimized and crystal structures for the reduced complexes. Even if the $Cu—S_{Met}$ bond does not become longer than 248 pm, this will decrease the energy difference between the optimized and crystal structures (i.e. below 4 kJ/mol). Furthermore, we have seen that increasing the basis set, the model size, or improving the theoretical method [15] also elongated the $Cu—S_{Met}$ bond, as did the dynamic effects at ambient temperature [61]. Inclusion of hydrogen bonds to the Cys ligand (as in the crystal structures) also elongates this bond by 15 pm [62]. If all these corrections are added together, the $Cu—S_{Met}$ bond length should become around 285 pm, i.e. close to the value observed in crystal structures (287–292 pm) [15]. Therefore, it is not clear if there is any discrepancy at all between the calculated and experimental length of this bond, but if there is any, it is very small in energy terms.

We tried to do similar calculations for the oxidized complexes, but owing to problems with the quantum chemical software, these have so far been without success.

4 Concluding remarks

The present calculation show that our original model structures of the blue copper proteins [15, 16] are reliable. Improvements of the basis sets and the model system do not change the structures significantly. Moreover, the two effects seem to cancel partly. Similarly, solvation seems to have a minor effect on the structure of the copper site; however, for the very flexible $Cu—S_{Met}$ bond, the effects are larger and they go in the same direction, i.e. to elongate the bond. Taken together with the dynamic effects at ambient temperatures (which also tend to elongate this bond [16]) these effects may explain the discrepancy between theoretical and experimental structures.

The results for the largest oxidized model **2** $[Cu(ImCH_3)_2(SC_2H_5)(S(CH_3)(C_2H_5))^+]$ are particularly interesting. This is the first realistic model for which both the trigonal and tetragonal structures are local minima. Therefore, we can estimate the relative stability of these two structures. Unfortunately, the energy difference is extremely small, only 2.5 kJ/mol. Even if the trigonal structure is more stable with this model, the difference is smaller than the uncertainty of the theoretical method. Therefore, we can still not decide which is the inherently stable structure of the blue copper site, but it is clear that the energy difference is extremely small.

In conclusion, improving the calculations led to structures that are a little, but significantly, more similar to the experimental structures, thereby making the discrepancy between theory and experiments smaller. In particular, we still see no evidence that the metal site of the blue copper proteins should be more strained than any other metal site (or ligand) in a protein. Neither have we seen any evidence for strain playing a role for the function of these proteins, for example, for the reorganization energies [27].

Acknowledgements. This investigation was supported by grants from the Swedish Natural Science Research Council. It was also supported by computer resources of the Swedish Council for Planning and Coordination of Research, Paralleldatorcentrum at the Royal Institute of Technology, Stockholm, and Lunarc at Lund university. A.C.B. acknowledges the continuous academic support by the Conselho Nacional de Desenvolvimento Cientifico e Technológio and Fundação de Amparo à Pesquisa do Estado de São Paulo, and the services and computer time at the Laboratório de Computação Cientifica Avançada at Universidade de São Paulo and Centro Nacional de Processamento de Alto Desempenho.

References

1. Sykes AG (1990) Adv Inorg Chem 36: 377
2. Adman T (1991) Adv Protein Chem 42: 145
3. Messerschmidt A (1998) Struct Bond 90: 37
4. Guss JM, Bartunik HD, Freeman HC (1992) Acta Crystallogr B 48: 190
5. Gray HB, Williams RJP, Malmström (2000) J Biol Inorg Chem 5: 551
6. Shepard WEB, Anderson BF, Lewandoski DA, Norris GE, Baker EN (1990) J Am Chem Soc 112: 7817
7. Marcus RA, Sutin NW (1985) Biochim Biophys Acta 811: 265
8. Williams RG (1963) In: Desnuelle PAE (ed) Molecular basis of enzyme action and inibition. Pergamon, Oxford, p 133
9. Malmström BG (1965) In: King TE, Mason HS, Morrison M (eds) Oxidases and related redox systems, vol 1. Wiley, New York, p 207
10. Vallee BL, Williams RJP (1968) Proc Natl Acad Sci USA 59: 498
11. Williams RJP (1995) Eur J Biochem 234: 363
12. Gray HB, Malmström BG (1983) Comments Inorg Chem 2: 203
13. Malmström BG (1994) Eur J Biochem 223: 711
14. Guckert JA, Lowery MD, Solomon EI (1995) J Am Chem Soc 117: 2817
15. Ryde U, Olsson MHM, Pierloot K, Roos BO (1996) J Mol Biol 261: 586
16. De Kerpel JOA, Pierloot K, Ryde U, Roos BO (1998) J Phys Chem B 102: 4638
17. Solomon EI, Penfield KW, Gewirth AA, Lowery MD, Shadle SE, Guckert JA, LaCroix LB (1996) Inorg Chim Acta 243: 67
18. Penfield KW, Gewirth AA, Solomon EI (1985) J Am Chem Soc 107: 4519
19. Gewirth AA, Solomon EI (1988) J Am Chem Soc 110: 3811
20. Larsson S, Broo A, Sjölin L (1995) J Phys Chem 99: 4860
21. LaCroix LB, Shadle SE, Wang Y, Averill BA, Hedman B, Hodgson KO, Solomon EI (1996) J Am Chem Soc 118: 7755
22. LaCroix LB, Randall DW, Nersissian AM, Hoitink CWG, Canters GW, Valentine JS, Solomon EI (1998) J Am Chem Soc 120: 9621
23. Gewirth AA, Cohen SL, Schugar HJ, Solomon EI (1987) Inorg Chem 26: 1133

24. Pierloot K, De Kerpel JOA, Ryde U, Roos BO (1997) J Am Chem Soc 119: 218
25. Pierloot K, De Kerpel JOA, Ryde U, Olsson MHM, Roos BO (1998) J Am Chem Soc 120: 13 156
26. Olsson MHM, Ryde U, Roos BO, Pierloot K (1998) J Biol Inorg Chem 3: 109
27. Olsson MHM, Ryde U, Roos BO (1998) Protein Sci 7: 2659
28. Olsson MHM, Ryde U (1999) J Biol Inorg Chem 4: 654
29. Ryde U, Olsson MHM, Roos BO, De Kerpel JOA, Pierloot K (2000) J Biol Inorg Chem 5: 565
30. Ryde U, Olsson MHM, Pierloot K (2001) In: Eriksson L (ed) Theoretical biochemistry, processes and properties of biological systems. Elsevier, Amsterdam p 1
31. Malmström BG, Leckner J (1998) Curr Opin Chem Biol 2: 286
32. Holm RH, Kennepohl P, Solomon EI (1996) Chem Rev 96: 2239
33. Treutler D, Ahlrichs R (1995) J Chem Phys 102: 346
34. Hertwig RH, Koch W (1997) Chem Phys Lett 268: 345
35. Schäfer A, Huber C, Ahlrichs R (1994) J Chem Phys 100: 5829
36. Hehre WJ, Radom L, Schleyer PVR, Pople JA (1986) In: Ab initio molecular theory. Wiley-Interscience, New York, p 133
37. Becke AD (1988) Phys Rev A 38: 3098
38. Perdew JP (1986) Phys Rev B 33: 8822
39. Slater JC (1974) Quantum theory of molecules and solids, vol 4: the self-consistent field for molecules and solids. McGraw-Hill, London
40. Vosko SH, Wilk L, Nusair M (1980) J Chem Phys 58: 1200
41. Bauschlicher CW (1995) Chem Phys Lett 246: 40
42. Eichkorn K, Treutler O, Öhm H, Häsen M, Ahlrichs R (1995) Chem Phys Lett 240: 283
43. Roos BO (1987) In: Lawley KP (ed) Advances in chemical physics; ab initio methods in quantum chemistry – II. Wiley, Chichester, p 399
44. Andersson K, Malmqvist P-Å, Roos BO, Sadlej AJ, Wolinski K (1990) J Phys Chem 94: 5483
45. Andersson K, Malmqvist P-Å, Roos BO (1992) J Chem Phys 96: 1218
46. Roos BO, Andersson K, Fülscher MP, Malmqvist P-Å, Serrano-Andrés L, Pierloot K (1996) In: Prigogine I, Rice SA (eds) Advances in chemical physics: new methods in computational quantum mechanics, vol XCIII. Wiley, New York, pp 219–331
47. Andersson K, Blomberg MRA, Fülscher MP, Karlström G, Lindh R, Malmqvist P-Å, Neogrády P, Olsen J, Roos BO, Sadlej AJ, Schütz M, Seijo L, Serrano-Andrés L, Siegbahn PEM, Widmark PO (1997) MOLCAS, version 4.0. Department of Theoretical Chemistry, University of Lund, P.O.B. 124, 221 00 Lund, Sweden
48. Widmark P-O, Malmqvist P-Å, Roos BO (1990) Theor Chim Acta 77: 291
49. Pierloot K, Dumez B, Widmark PO, Roos BO (1995) Theor Chim Acta 90: 87
50. Frisch MJ, Trucks GW, Schlegel HB, Scuseria GE, Robb MA, Cheeseman JR, Zakrazewski VG, Montgomery JA, Stratmann RE, Burant JC, Dapprich S, Milliam JM, Daniels AD, Kudin KN, Strain MC, Farkas O, Tomasi J, Barone V, Cossi M, Cammi R, Mennucci B, Pomelli C, Adamo C, Clifford S, Ochterski J, Petersson GA, Ayala PY, Cui Q, Morokuma K, Malick DK, Rabuck AD, Raghavachari K, Foresman JB, Cioslowski J, Ortiz JV, Stefanov BB, Liu G, Liashenko A, Piskorz P, Komaromi I, Gomperts R, Martin RL, Fox DJ, Keith T, Al-Laham MA, Peng CY, Nanayakkara A, Gonzalez C, Challacombe M, Gill PMW, Johnson B, Chen W, Wong MW, Andres JL, Head-Gordon M, Replogie ES, Pople JA (1998) Gaussian 98, revision A.5. Gaussian, Pittsburgh, PA
51. Tomasi J, Persico M (1994) Chem Rev 2027
52. Barone V, Cossi M (1998) J Phys Chem A 102: 1995
53. Periotti RA (1976) Chem Rev 717
54. Floris FM, Tomasi J (1989) J Comput Chem 10: 616
55. Floris FM, Tomasi J, Pascual-Ahuir JL (1991) J Comput Chem 12: 784
56. Barone V, Cossi M, Tomasi J (1997) J Chem Phys 107: 3210
57. Ryde U (1999) Biophys J 77: 2777
58. Sharp KA (1990) Annu Rev Biophys Biophys Chem 19: 301
59. Rodgers KK, Sligar SG (1991) J Am Chem Soc 113: 9419
60. Honig B Science, (1995) 268: 1144
61. Warshel A (1991) Computer modelling of chemical reactions in enzymes. Wiley, New York
62. Ryde U, Olsson MHM (2000) Int J Quantum Chem Biophys (in press)
63. Adman ET, Godden JW, Turley S (1995) J Biol Chem 270: 27 458
64. Nar H, Messerschmidt A, Huber R, van der Kamp M, Canters GW (1991) J Mol Biol 218: 427